ON JET FORMATION VS. PROPAGATION AND EXPERIMENTS

Eric Blackman (UR)

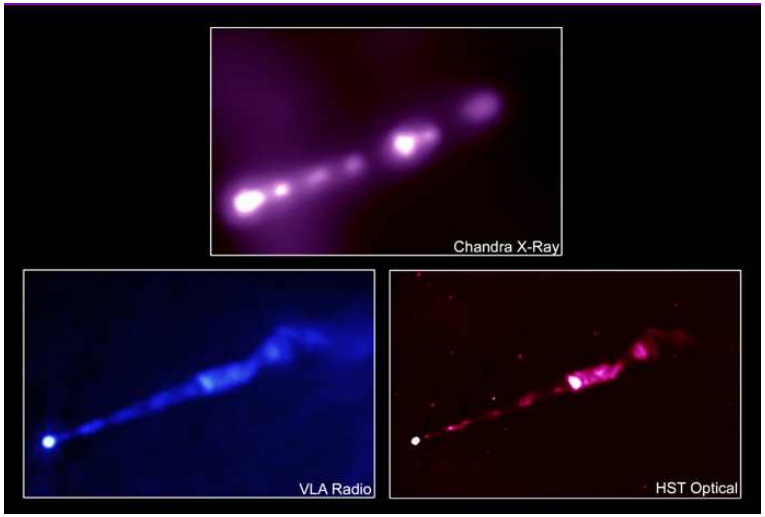

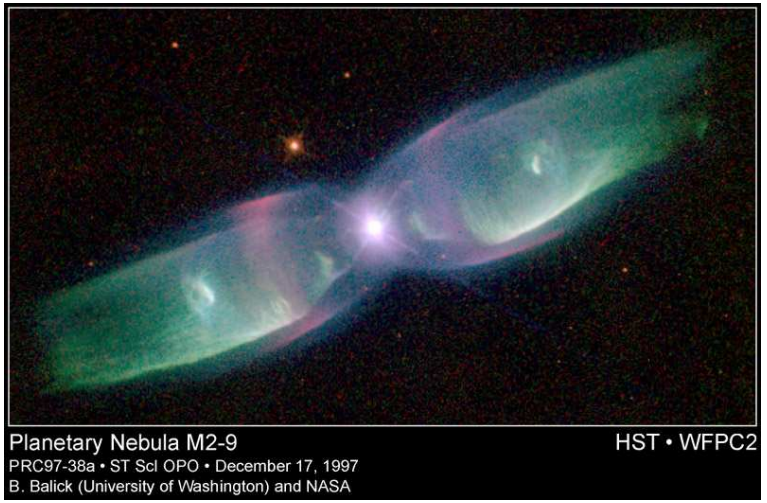

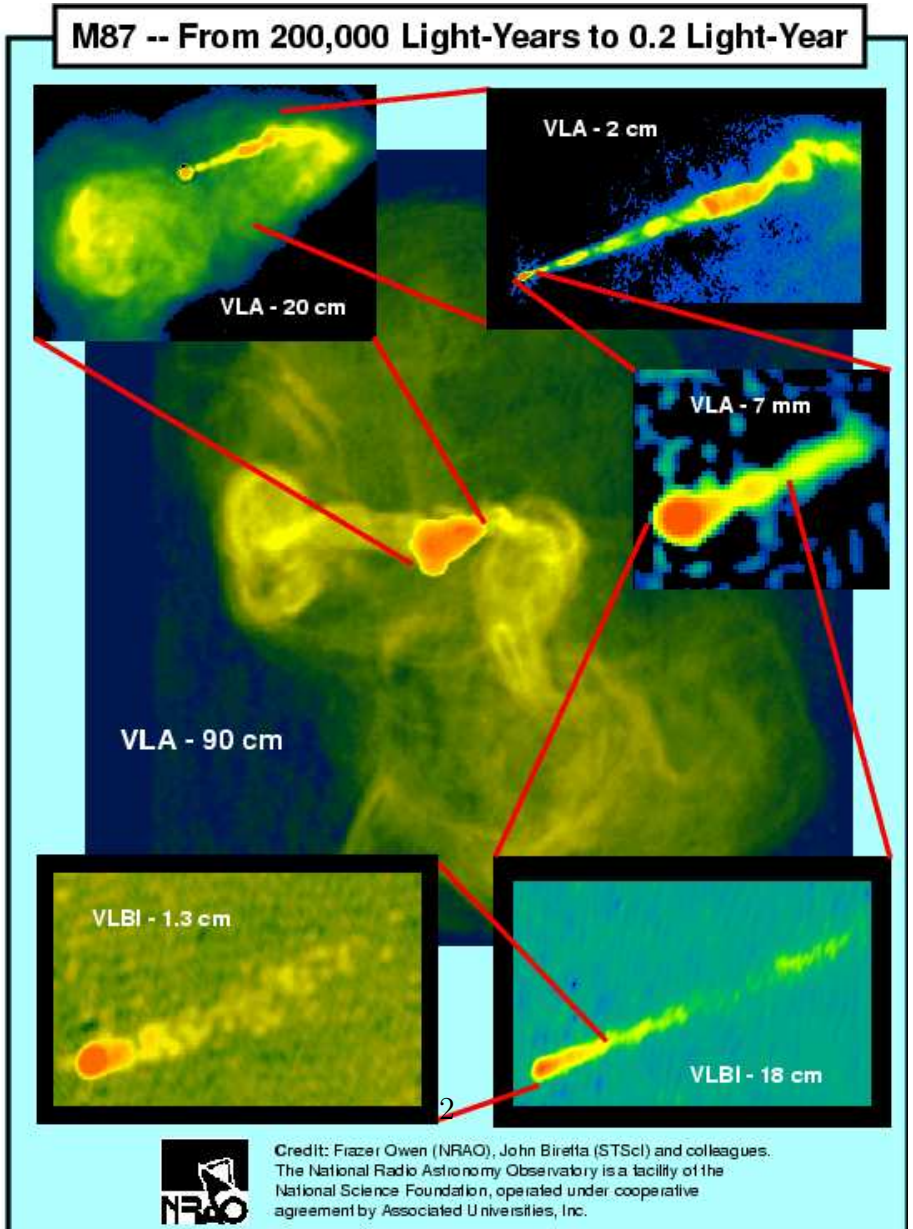
M87 -- From 200,000 Light-Years to 0.2 Light-Year
VLA - 2 cm
VLA - 20 cm
VLA - 7 mm
VLA - 90 cm
VLBI - 1.3 cm
VLBI - 18 cm
Credit: Frazer Owen (NRAO), John Biretta (STScI) and colleagues.
The National Radio Astronomy Observatory is a facility of the
National Science Foundation, operated under cooperative
agreement by Associated Universities, Inc.

LAUNCH vs. COLLIMATION vs. PROPAGATION

• Asymptotic propagation: ($r \gtrsim 100 R_{obj}$) vs. launch region ($r \lesssim 50 R_{obj}$)

• Observations resolve scales $r > 50 R_{obj}$. Need microarcsec resolution to study launch region. Current resolution in radio: at 0.1-1 milliarcsec.

• *Theoretical* "consensus" that B-fields are dominant in launch region ($r \lesssim 50 R_{obj}$) for all *formidable* astrophysical jets.

• Observations *indirectly* support or do not refute this theoretical consensus

• "Best" evidence for MHD launch: rotation in YSO jets $\lesssim$ 100 AU scales. (Bacciotti et al. 2002-05; Coffey et al. 2004,2005; Woitas et al. 2004)

• Does B dominate in propagation region at $r > 50 r_{obj}$?
→ YSO and PNe jets: probably flow dominated at $r >$ 100AU

→ AGN (galactic BH engine) and GRB, Microquasar (stellar BH engines) might be B-dominated to large r but how far from engine?

• YSO jets (overdense, non-rel.) vs. AGN/GRB/MQ jets (underdense, rel.)

MAGNETIC FLING/ STEADY

(figs from Shu et al. 94; Pelletier & Pudritz 92)

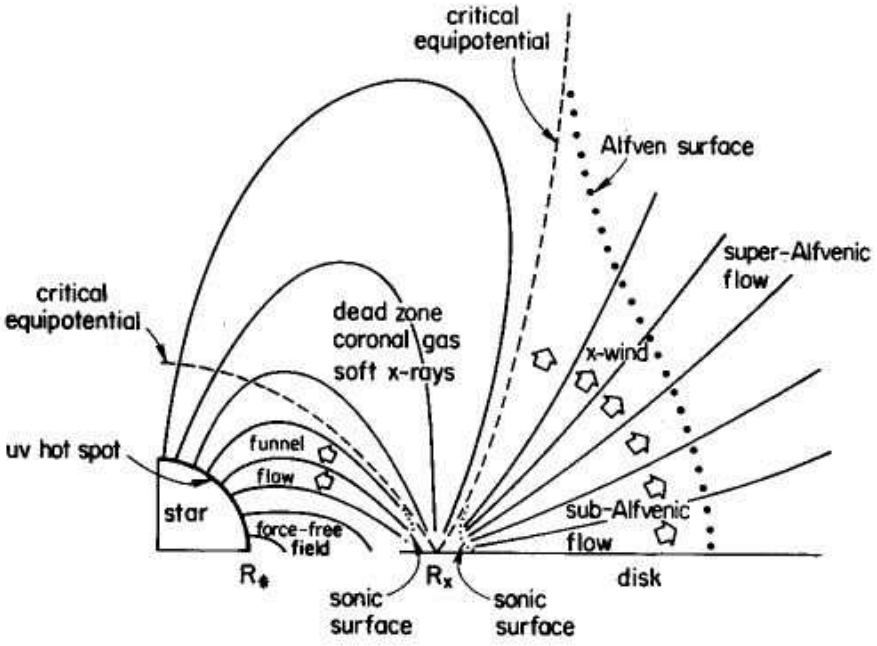

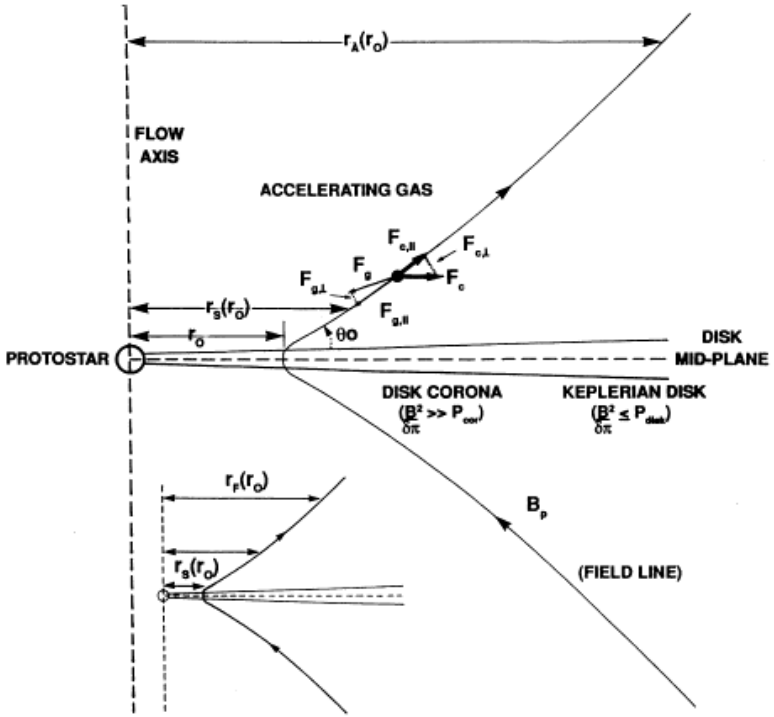

MAGNETIC SPRING EXPLOSION/ TIME-DEPENDENT

(picture from Meier et al. 01; Matt et al. 03; 05)

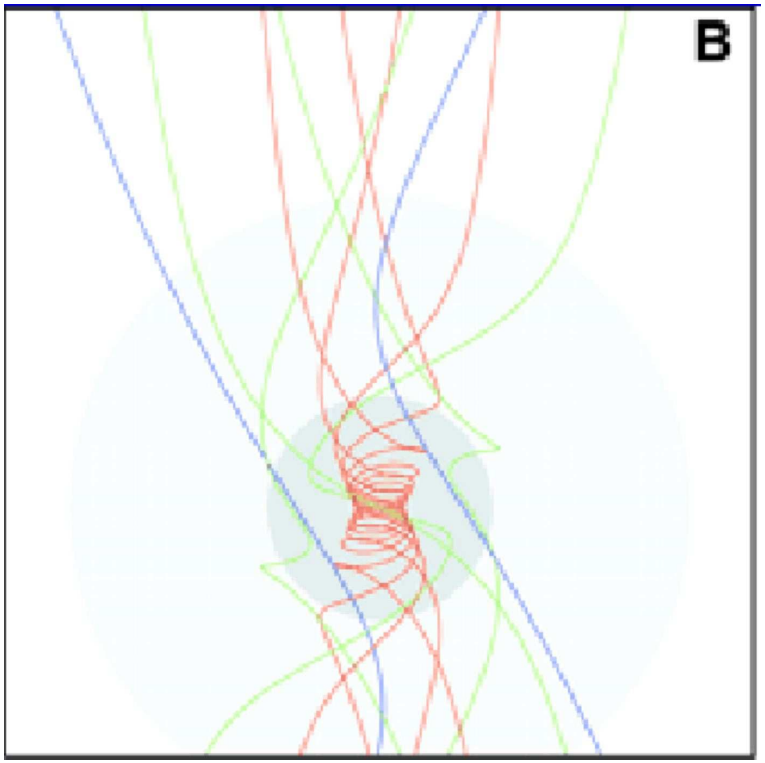

POYNTING FLUX DOMINATED OR HYBRID

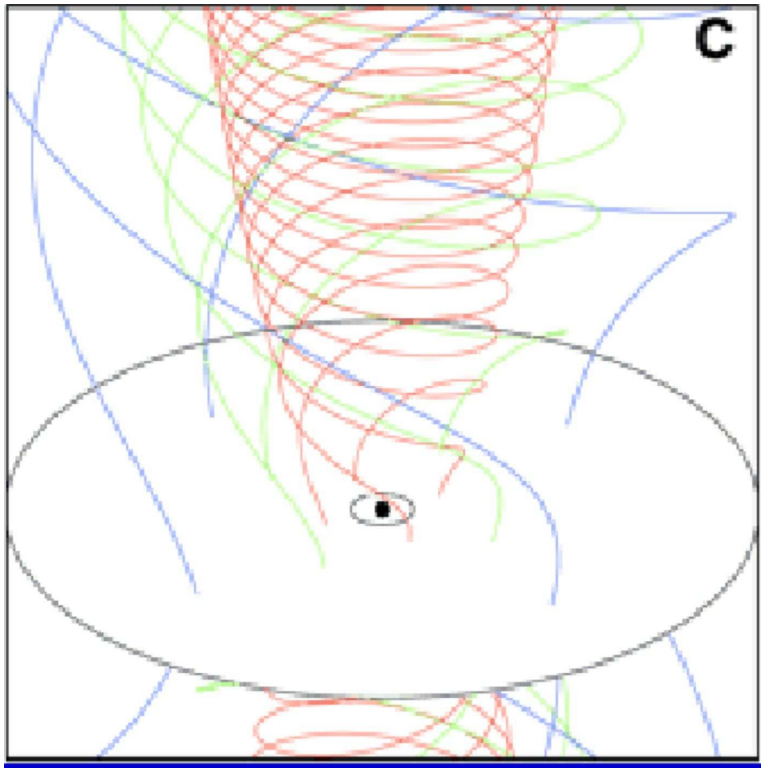

SUN PROVIDES INSIGHT INTO LAUNCH REGION

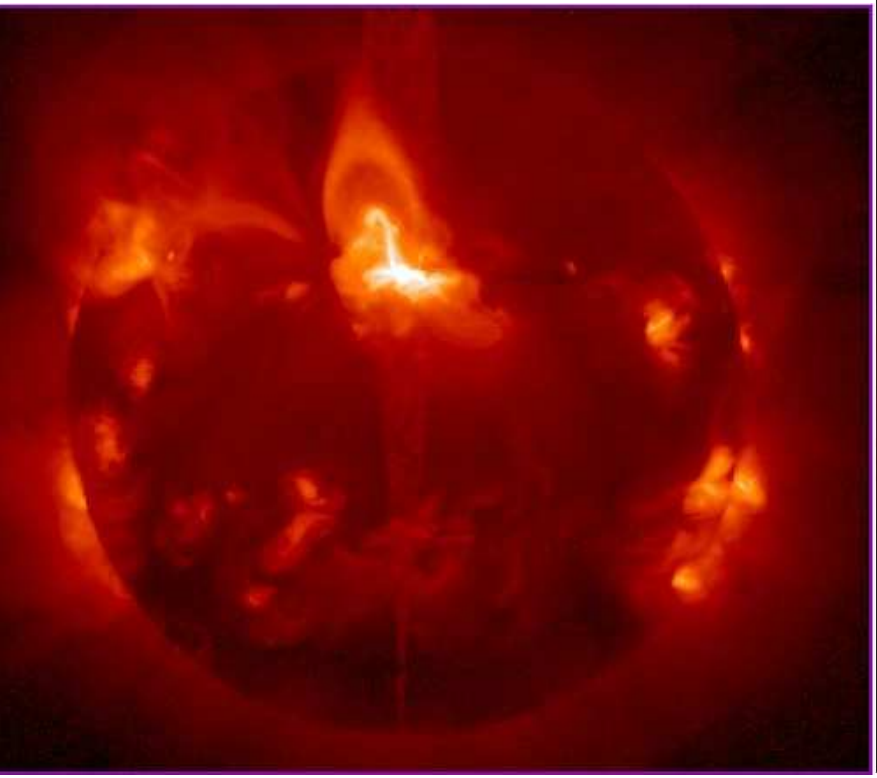

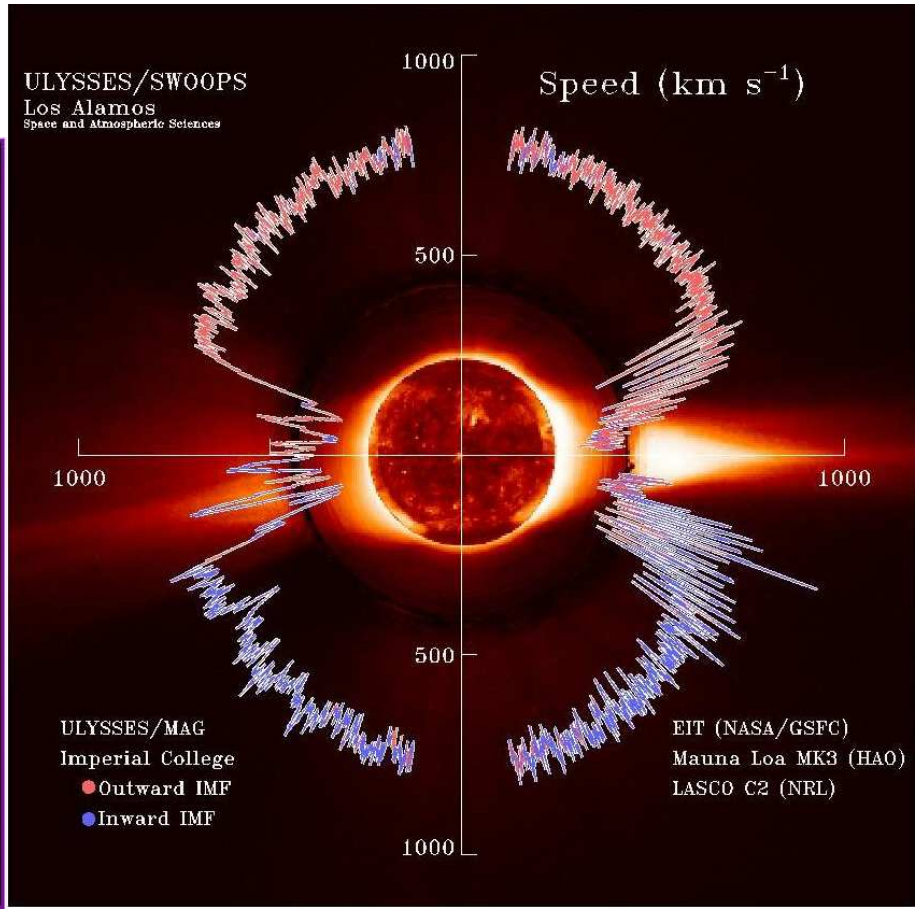

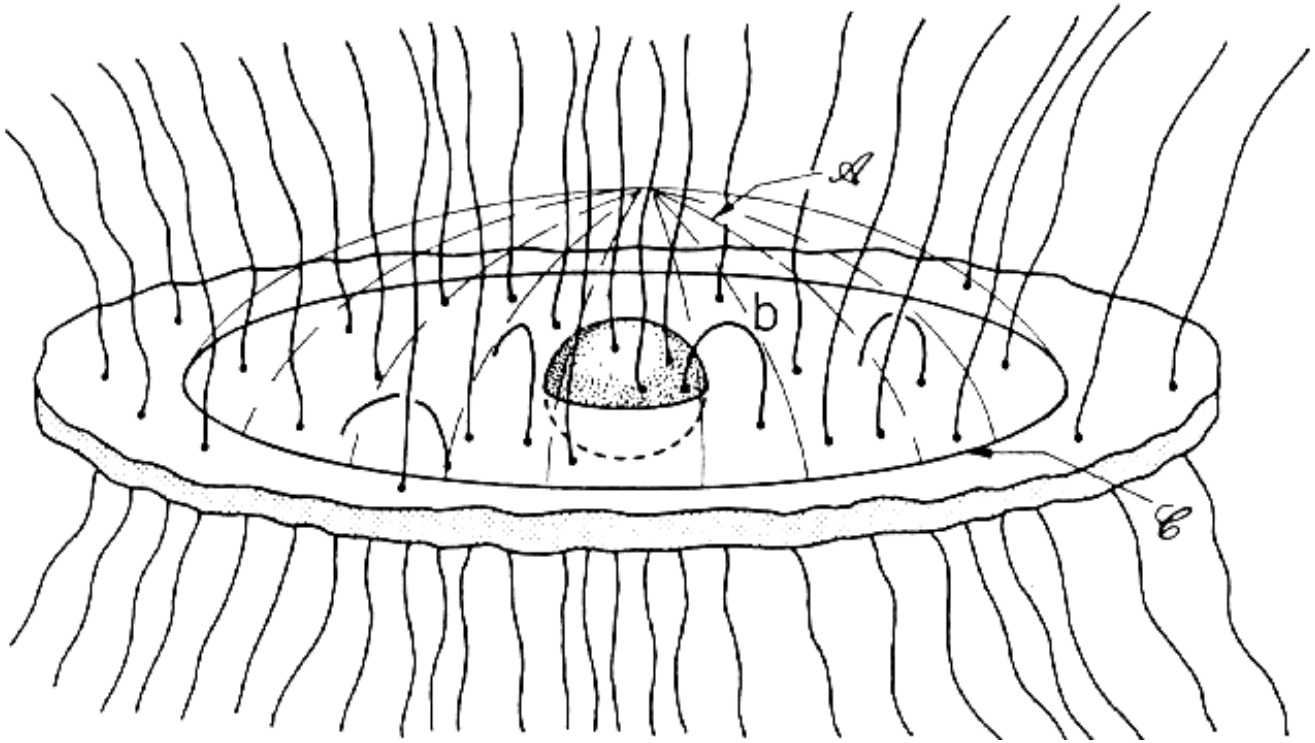

(Thorne et al. 1986)

LAUNCH REGION: DISKS, CORONAL HOLES & LARGE SCALE B GROWTH

- **In large scale field production is helpful, if not essential**

Disks:

(1) Poloidal flux freezing in thin disks not guaranteed

(2) **B**-field to corona requires $t_{dif} > t_{buo} \rightarrow$ favors larger scales

Stars:

(1) Solar cycle shows flux is not frozen in sun

(2) Helical dynamo overcomes turbulent diffusion

3 TYPES OF DYNAMOS IN ASTROPHYSICS

Small Scale Velocity Driven Dynamo:

- field amplification on scales **at or smaller** than largest turbulent scale
- $\overline{\boldsymbol{\mathcal{E}}}_{||} = \langle \mathbf{v} \times \mathbf{b} \rangle$ can be zero
- Neither kinetic nor magnetic helicity required

Large Scale Velocity Driven Dynamo:

- field amplification on **scales larger** than the largest "turbulent" scale.
- $\overline{\boldsymbol{\mathcal{E}}}_{||} \neq 0$ (mean pseudosalar or pseudovector required)
- magnetic helicity separator: pumps one sign to small, other to large scales
- accompanied by a velocity driven small scale dynamo
- saturation value explained by nonlinear mag. helicity evolution

Large Scale Mag. Driven Dynamo/ Mag. Relaxation (corona):

- Converts strong **B**-field from unrelaxed to relaxed configuration and sustains
- finite $\overline{\boldsymbol{\mathcal{E}}}_{||}$ (mean pseudosalar or pseudovector required)
- Magnetic helicity transferred from small to large scales
- Boundary of rotator to corona analagous to SPHEROMAK

PARADIGM FOR JET FIELDS (OR CORONAL HOLES):

(1) Velocity driven helical dynamo produces fields of large enough scale to make it to corona.

- Disk is helicity injecting bdry. to corona

(2) Dynamical relaxation (= magnetically dominated dynamo e.g. Blackman 05) in corona to open up fields to much larger global scales, e.g. for jets and coronal holes.

- also magnetic tower (e.g. Lynden-Bell; Uzdensky..)
- Above is similar to laboratory plasma devices (Spheromak/Tokomak)

IMPORTANT FOR JETS AND LAB EXPERIMENTS:

• For stars and accretion disks, we probe at best, the coronal field, or base of jet NOT the field growth in rotator.

• Paradigm implies that the dynamical relaxation stage of the field growth occurs at the base of jet: i.e. it is the formation stage of the jet.

• **disk interior** vs. **jet formation in corona** vs. **jet propagation** regimes

What should we expect from jet experiments?

- Physics pieces of the puzzle; not reproduction of astrophysical object
- Code testing/benchmarking.
- Physical principles can be tested; but can we "solve" astrophysical problems?

time will tell

- We should be patient... (difficultites, diagnostic techniques improving, small time and spatial scales, only recent emergence of graduate students)
- Expts offer new windows using new tools which are improving.

– –

Hsu & Bellan 2002 MNRAS (Spheromak, magnetic jet formation, MHD kink)
Lebedev et al. 2005 MNRAS (Pulsed power radial array, MHD tower)
Lebedev et al. 2004,ApJ 616, 988 (Pulsed power z-pinch, HD, crosswind)
Lebedev et al. 2002,ApJ 563,113 (Pulsed power z-pinch, HD, radiative cooling)
Blue et al. 2005,PRL 94, 095005 (NIF, Laser ICF, HD 2-D vs 3-D aperture)
Foster et al. 2005,ApJL 94, 095005 (OMEGA,Laser ICF, HD Jet/ shock)

Hsu Bellan 02 MAG.LAUNCH/CORONA EXP. (Spheromak)

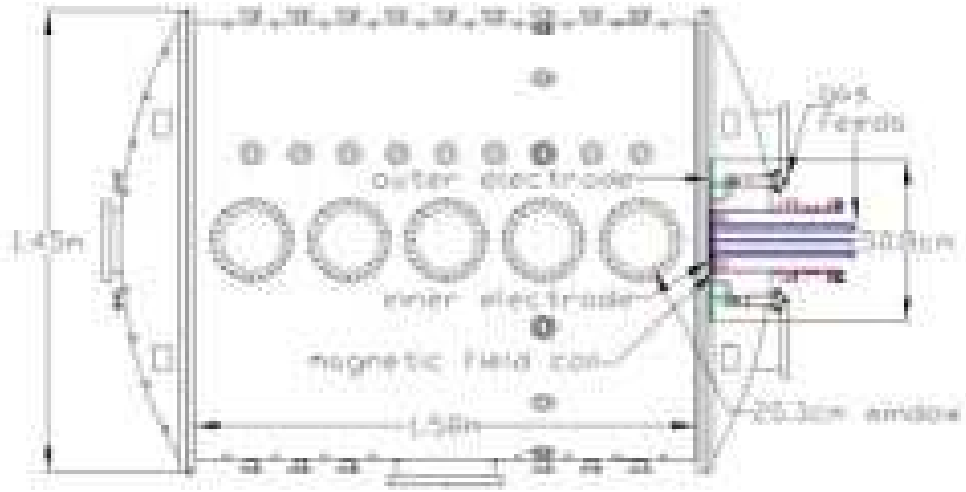

Figure 1. Side-view schematic of vacuum chamber and planar coaxial gun setup.

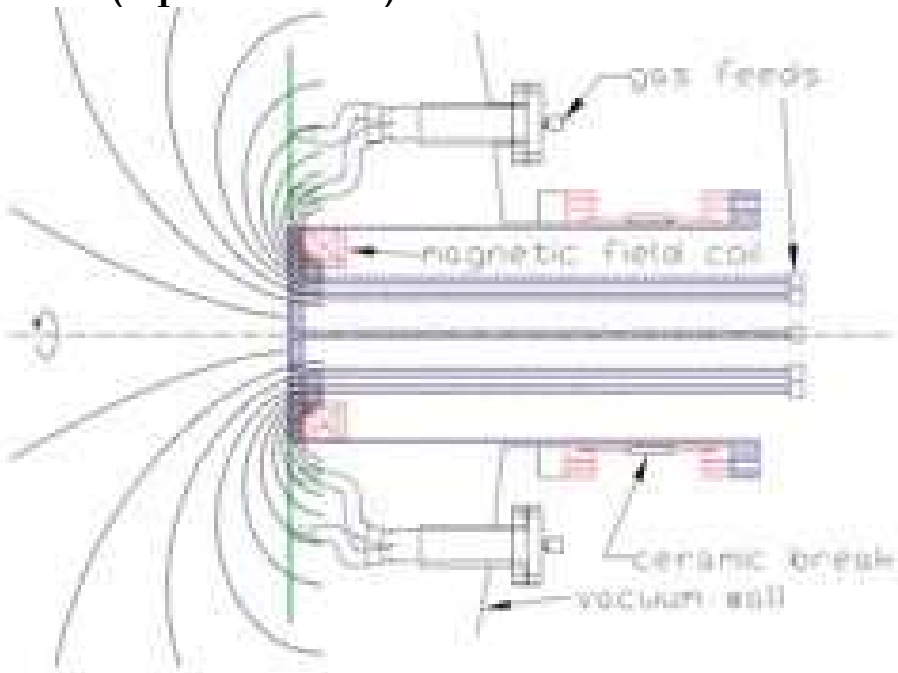

Figure 2. Side-view schematic of planar coaxial gun, including gas feeds, external magnetic field coil, poloidal flux ψ contours and symmetry axis.

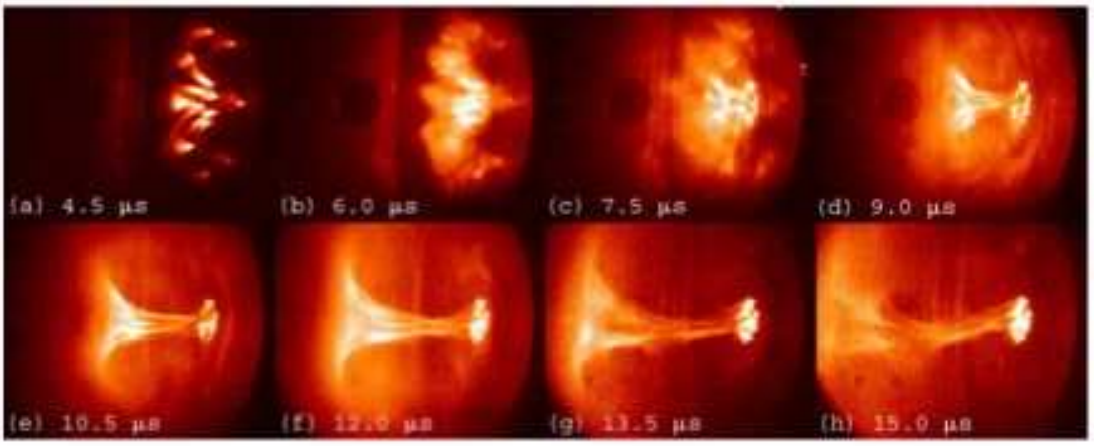

Figure 3. Images of plasma evolution (shot 1210; peak $\alpha_{\text{plat}} = 66\,\text{m}^{-1}$) in which a plasma column forms and persists for many Alfvén transit times, illustra the magnetic topology required for an astrophysical jet.

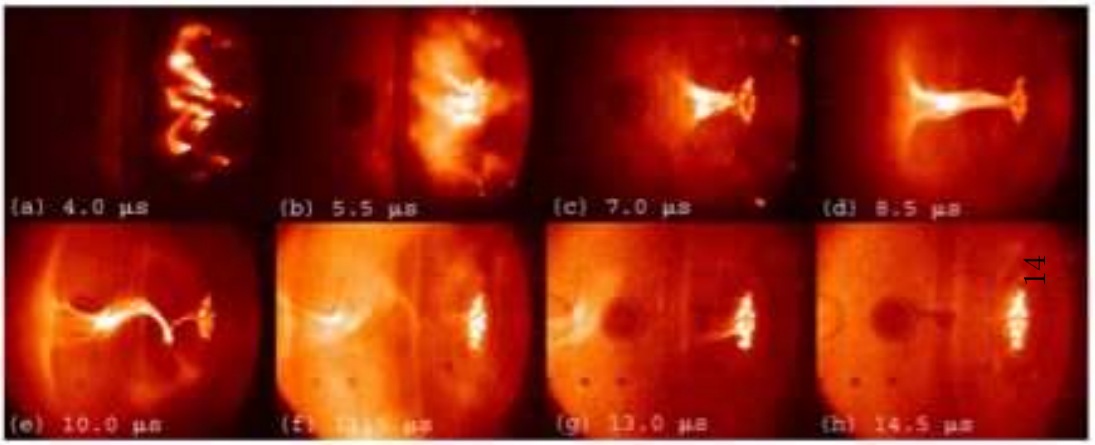

Figure 4. Images of plasma evolution (shot 1233; peak $\alpha_{\text{plat}} = 71\,\text{m}^{-1}$) in which a helical instability, probably a current-driven kink, develops on the MHD time-scale, illustrating one possible source of jet internal structure.

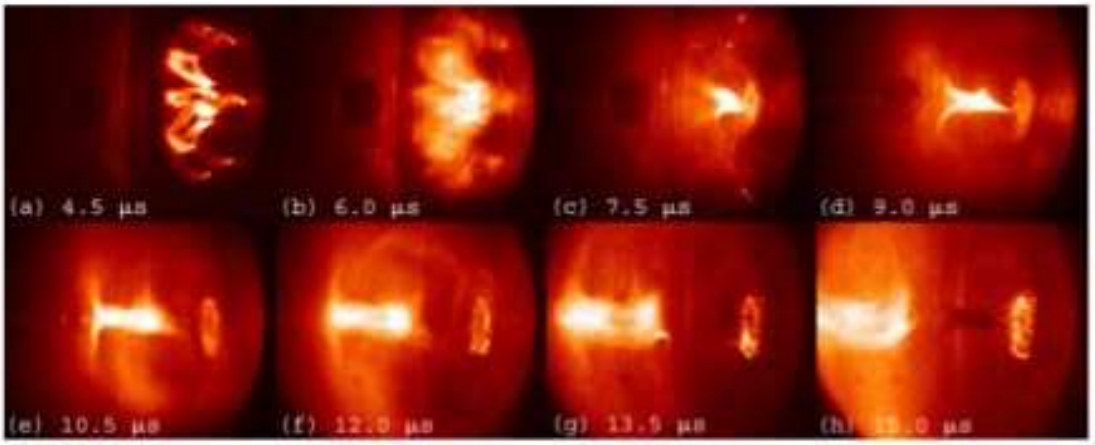

Figure 6. Images of plasma evolution (shot 1181; peak $\alpha_{\text{plat}} = 129\,\text{m}^{-1}$) in which the plasma detaches from the electrodes, illustrating the possibility of line opening in disc coronae.

• $\alpha_{inj} \equiv \mathbf{J} \cdot \mathbf{B}/B^2 = I/\psi \leq 4\pi/L \rightarrow$ stable tower formation (Hsu Bellan)

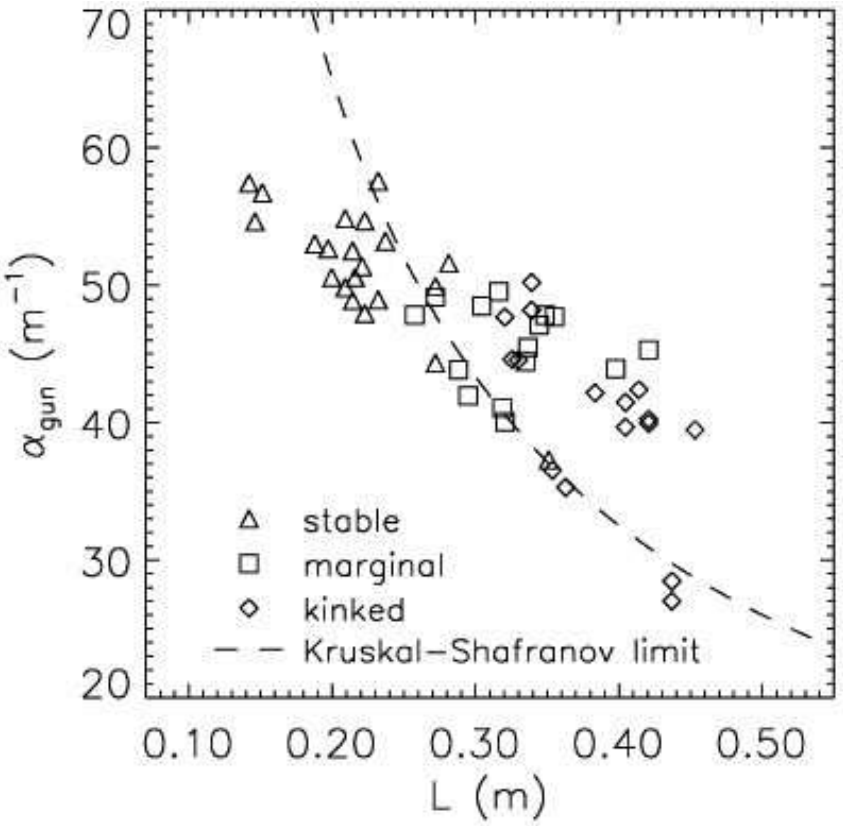

Figure 5. A plot of α_{gun} versus column length L for different plasmas, showing good agreement with the Kruskal–Shafranov condition for a current-driven kink instability.

Insights from Hsu Bellan 02 SPHEROMAK EXP.

• probes jet formation in $\beta \sim 0.02 - 0.1$ region (5-20eV, 1kG, $n = 10^{14}/cm^3$).

• (Alfvén) Mach number < 1

• Magnetic loops + potential drop (or shear) injects **magnetic helicity, current helicity**, and thus azimuthal field

• Evolution to relaxed state involves increase scale of field; **dynamical magnetic relaxation** toward "force free state"

• (plasma expansion and collimation from B_θ)

• Small $\alpha_{inj} \equiv \mathbf{J} \cdot \mathbf{B}/B^2 = I/\psi \leq 4\pi/L$: Stable tower formation

• Intermediate $\alpha_{inj} \gtrsim 4\pi/L$: Magnetic tower formation + Kink Instability

• Large $\alpha_{inj} >> 4\pi/L$: Magnetic tower formation + Kink Instability + Spheromak Formation (disconnected blob)

• Value of α_{inj} in real system determined by shear, resisitivity, coronal density.

Lebedev et al.05, MAGNETIC TOWER EXP (wire array/MAGPIE)

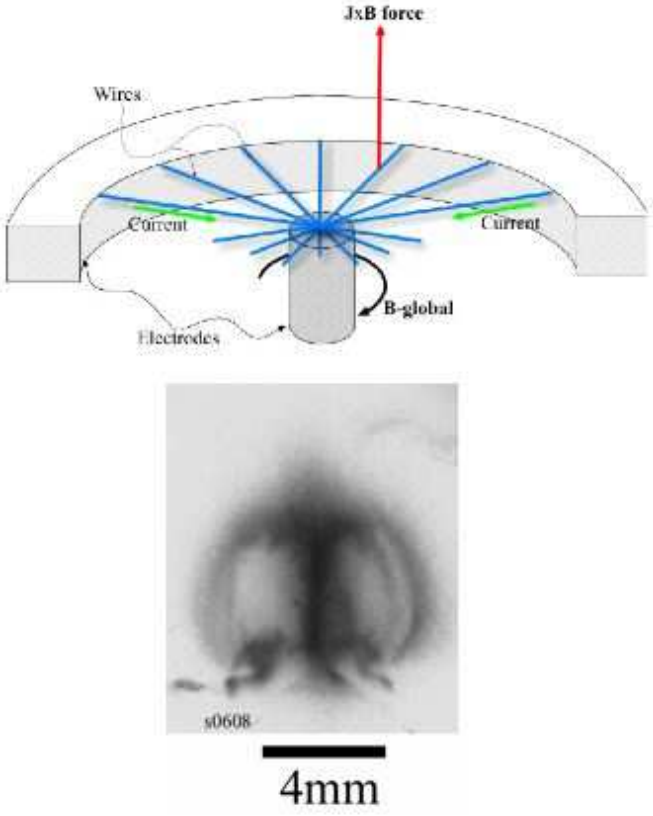

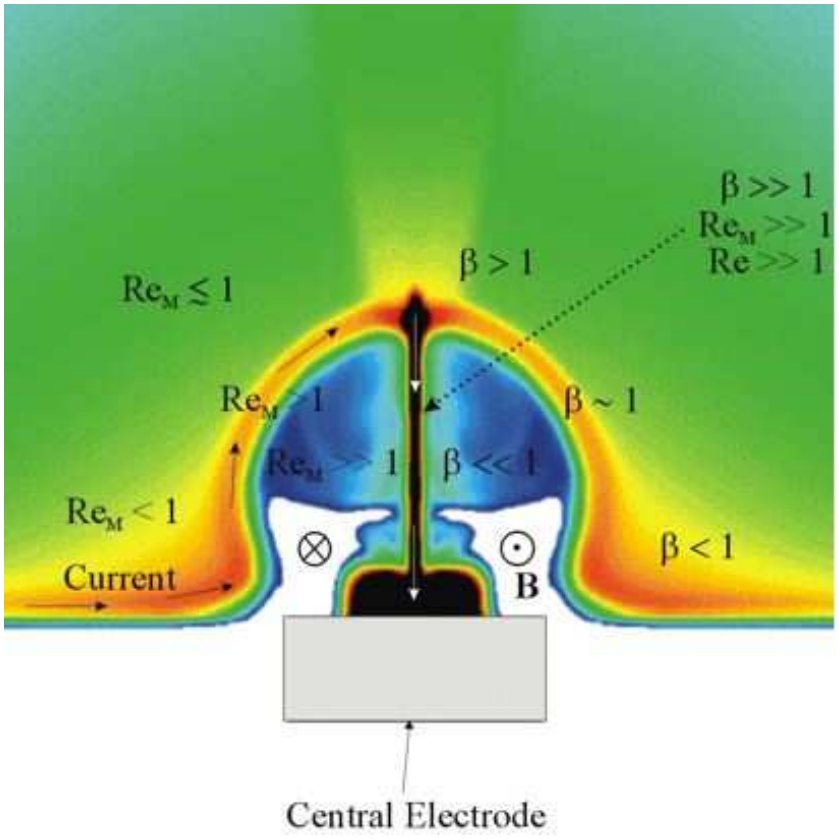

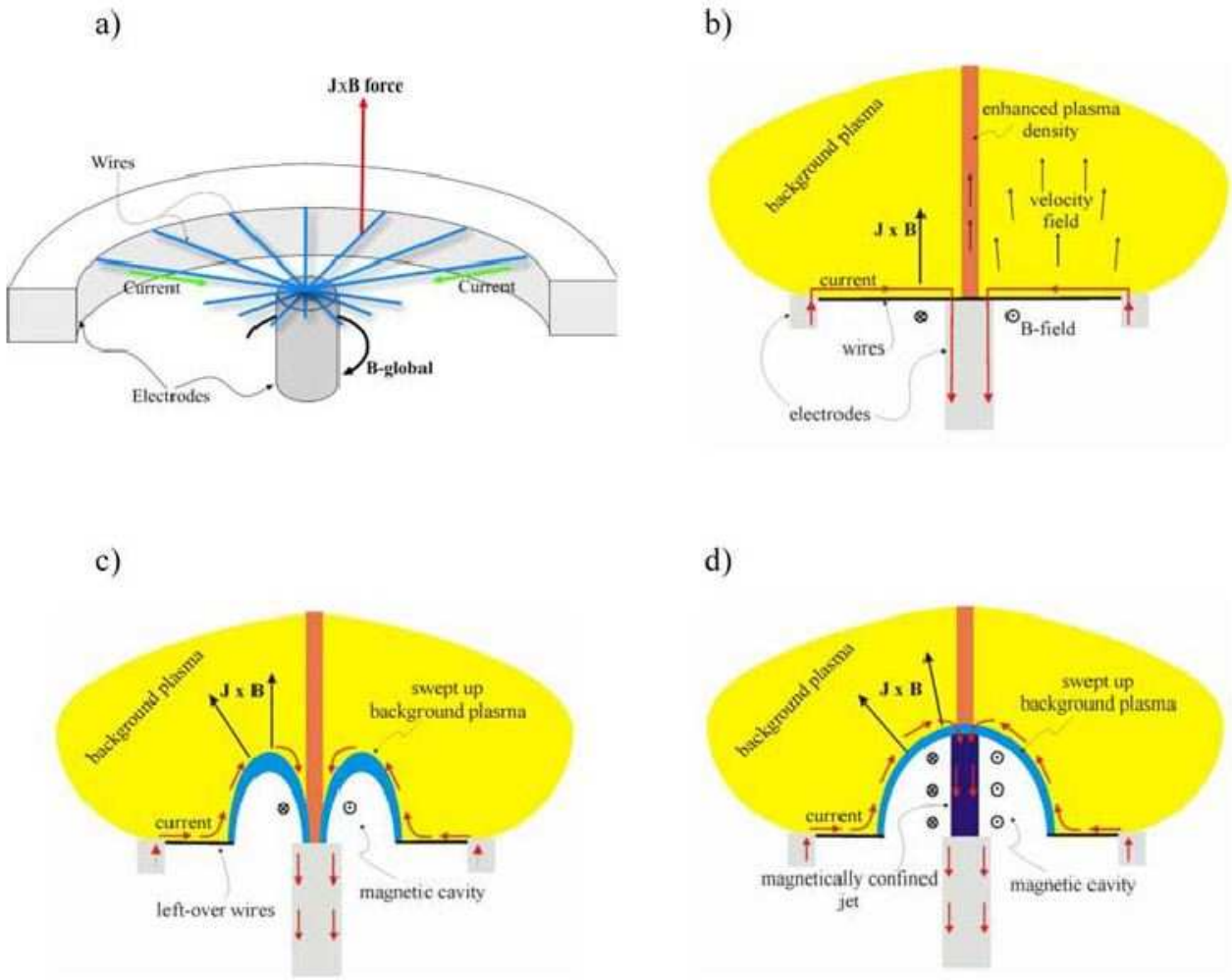

Figure 1. (a) Schematic of a radial wire array experiment. Currents flow radially through fine metallic wires and along the central electrode, producing a toroidal magnetic field which lies below the wires. (b) The $\boldsymbol{J} \times \boldsymbol{B}$ force acting on the plasma ablated from the wires produces a plasma background above the array, and because of resistive diffusion, the current path remains close to the wires. (c) Full ablation of the wires near the central electrode leads to formation of a magnetic cavity, which evolves (d) into a magnetic tower jet driven upwards by the pressure of the toroidal magnetic field.

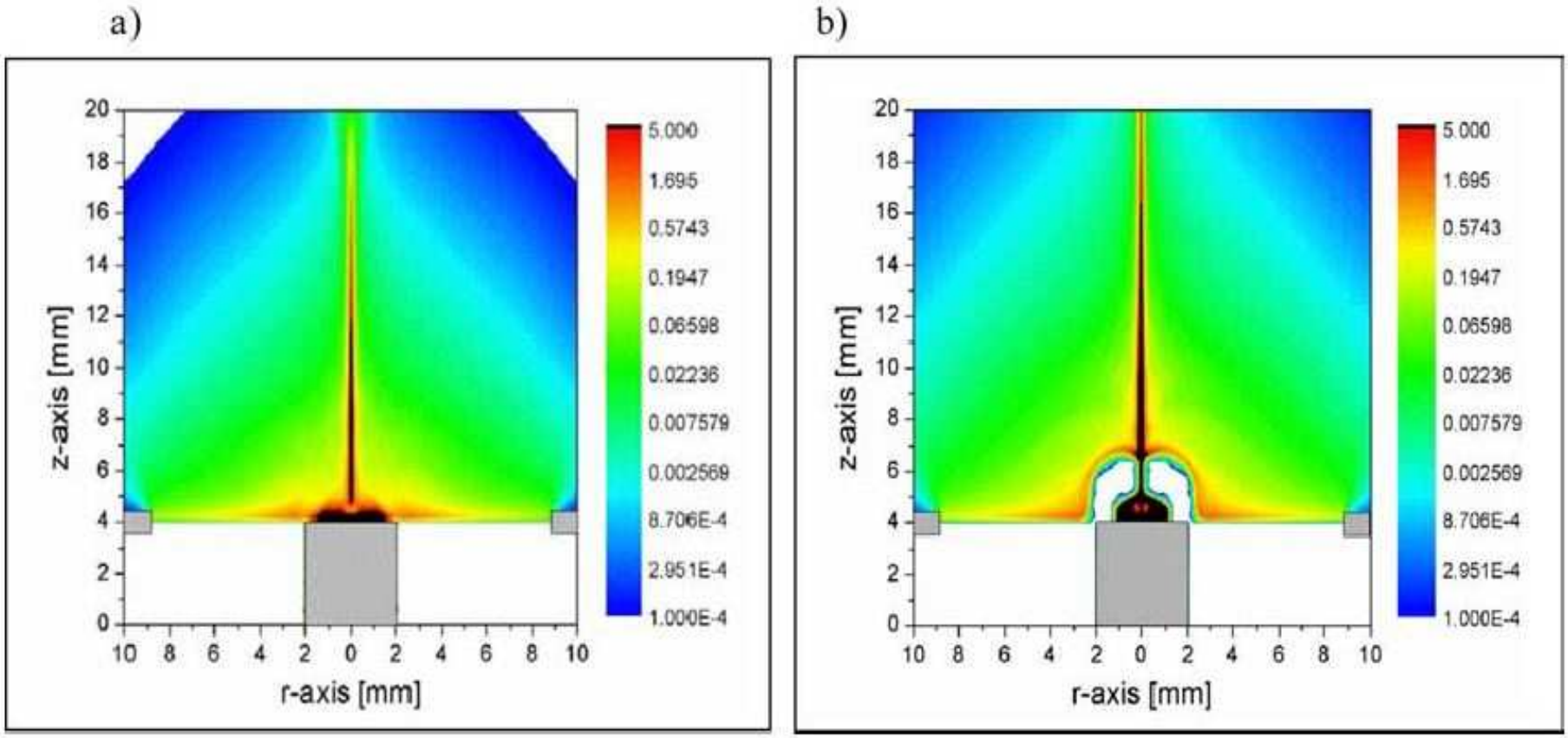

Figure 2. Axisymmetric, two-dimensional, resistive MHD simulations showing the spatial distribution of plasma mass density [kg m^{-3}] (a) before and (b) just after the beginning of magnetic cavity formation. The hatched areas indicate the position of the electrodes.

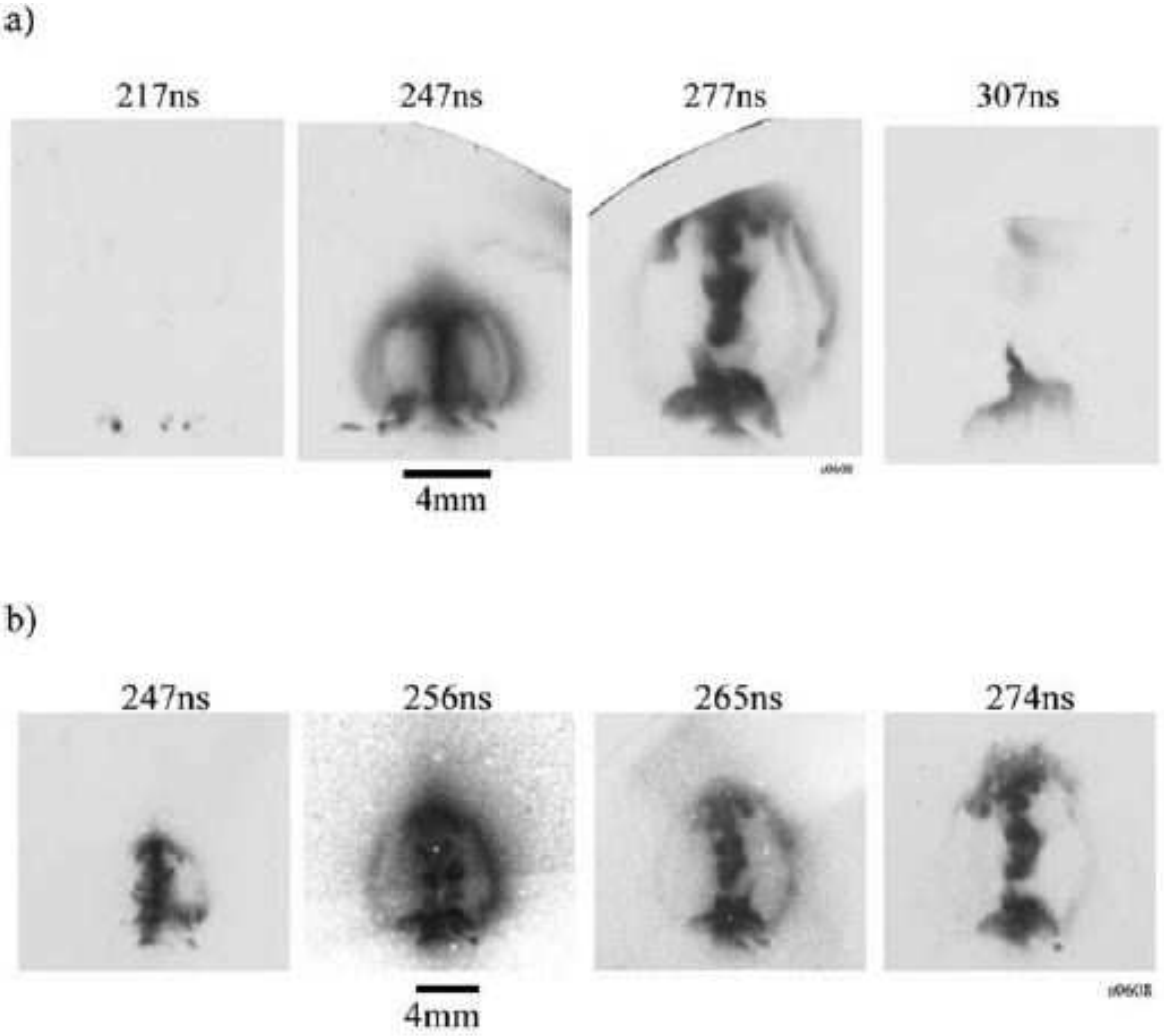

Figure 4. Time sequence of soft X-ray images obtained during the same experiment showing expansion of the magnetic cavity and development of instabilities in the central jet column. The four images in part (b) were taken with smaller interframe time separations and from different viewing angle.

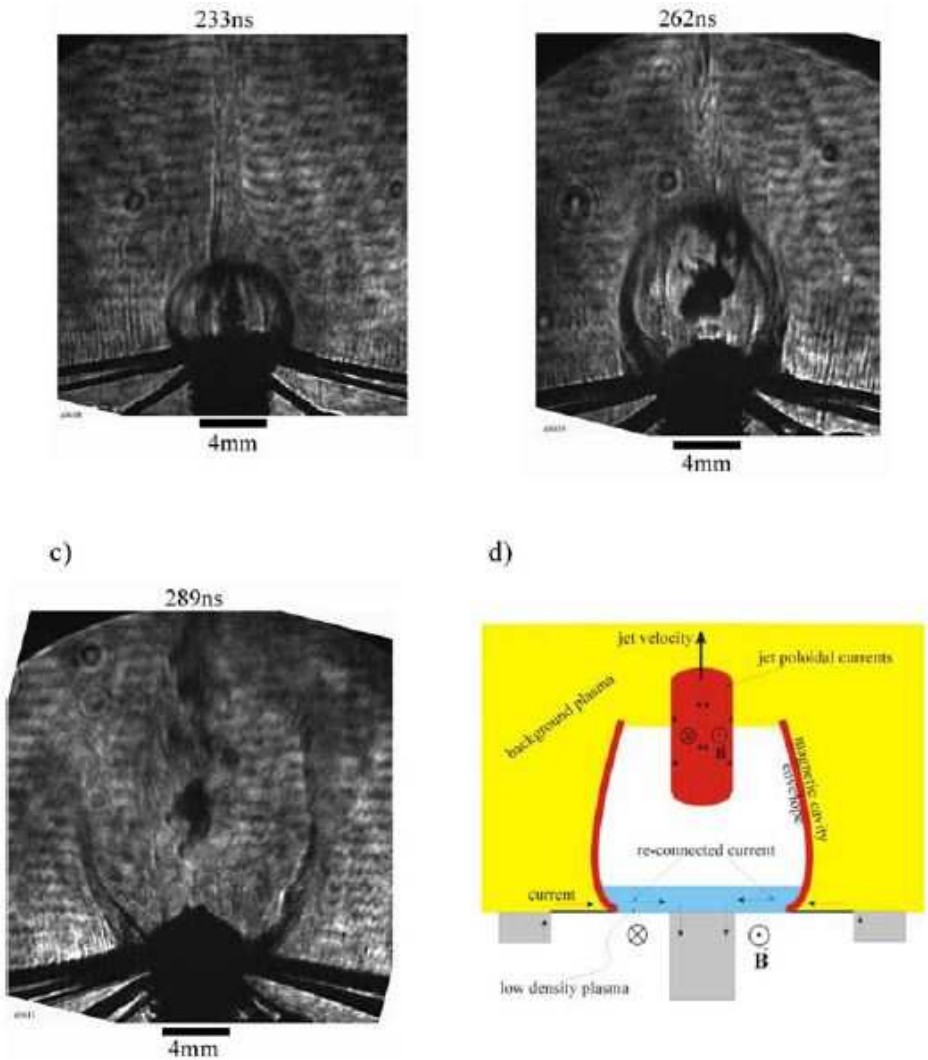

Figure 6. Laser shadowgraphs of the magnetic jet evolution. (a) At 233 ns the magnetic cavity is well developed. A collimated jet is clearly visible on-axis inside the cavity. (b) The magnetic cavity elongates axially and expands radially. Because of instabilities sections of the jet on-axis are no longer visible, and the jet assumes a clumpy structure. (c) The upper edge of the magnetic cavity breaks up and disappears. On-axis is still visible a well collimated clumpy jet. (d) Schematic of the last stage of the magnetic jet evolution, showing how currents reconnect at the foot-point of the magnetic tower and a jet is ejected with entrained magnetic fields.

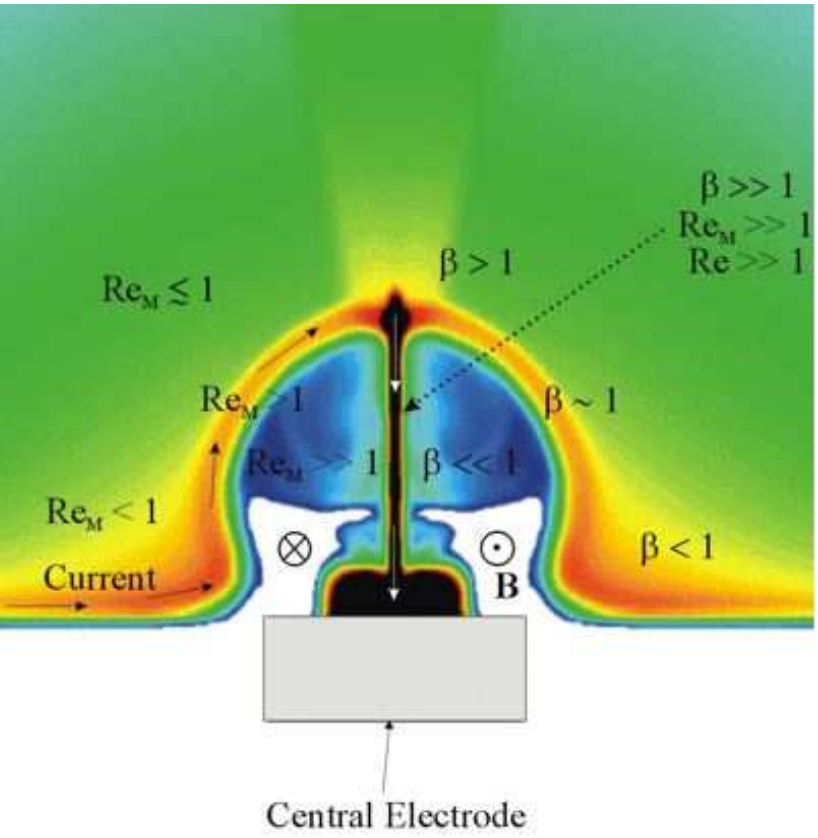

Characteristic physical conditions and dimensionless parameters in the jet and background plasma jet

Ion number density	n_i	10^{18}–10^{19}	cm^{-3}
Temperature	T	120	eV
Ionization	Z	20	
Velocity	v	100–200	km s^{-1}
Magnetic field strength	B	>500	kG
Mach number	M	3–5	
Magnetic Reynolds number	Re_M	~10	
Plasma β	β	~1	
Cooling parameter	χ	10^{-3}–10^{-4}	
Reynolds number	Re	$>10^4$	
Peclet number	Pe	5–20	
Background plasma			
Density	n_i	10^{16}–10^{17}	cm^{-3}
Temperature	T	<20	eV
Ionization	Z	10–15	
Sound speed	C_s	10–15	km s^{-1}
Magnetic field strength	B	<50	kG

Insights from Lebedev et al. 05 MAG. TOWER EXP.

- Probes jet formation and some aspects of propagation
- In situ formation of magnetic tower
- Toroidal magnetic pressure drives outflow
- Low β "force-free" magnetic tower beneath boundary
- Thermal pressure confines magnetic tower.
- Magnetically confined $\beta = 1$ core. (jet = core) (e.g. YSOs)
- Supersonic motion + cooling collimates precursor jet
- Return current evolves from base to tower boundary, back to base.
- Time dependent dynamics are important
- Disconnected bubbles due to instability
- Jet lasts 20 times longer than kink instability growth time ($\beta = 1$ jet core).
- Diagnostic techniques (Interferometry, probe shadowing, x-ray imaging)
- Symbiotic use/test of code and experiments
- Dimensionless parameters crudely OK for MHD astro-comparison

Lebedev et al.02, Hydrodynamic Propagation/Cooling (Z-pinch/MAGPIE)

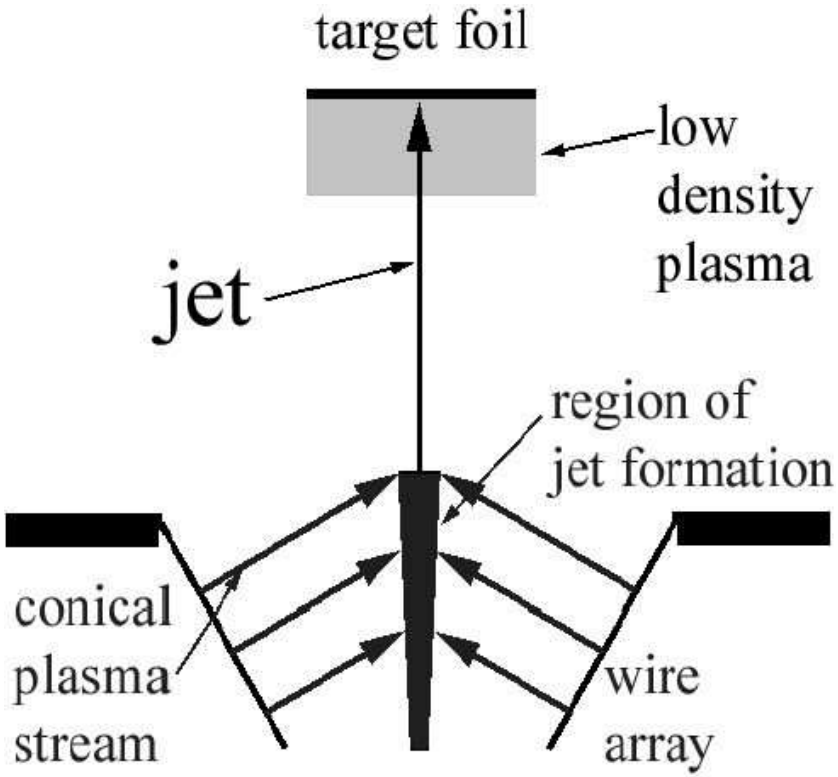

FIG. 1.—Schematic of the experiment

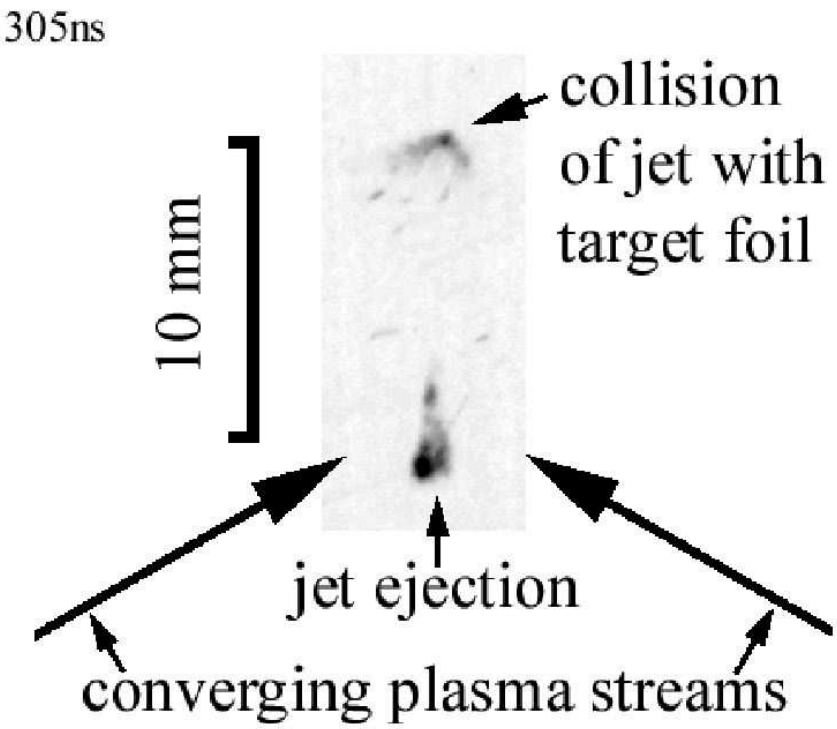

FIG. 4.—Time-resolved soft X-ray image showing interaction of the jet with thin plastic foil. Emission from the jet rapidly decays due to radi
as the jet leaves the formation region. Emission is seen again from the region where the jet is decelerated by the foil and kinetic energy is co
thermal energy.

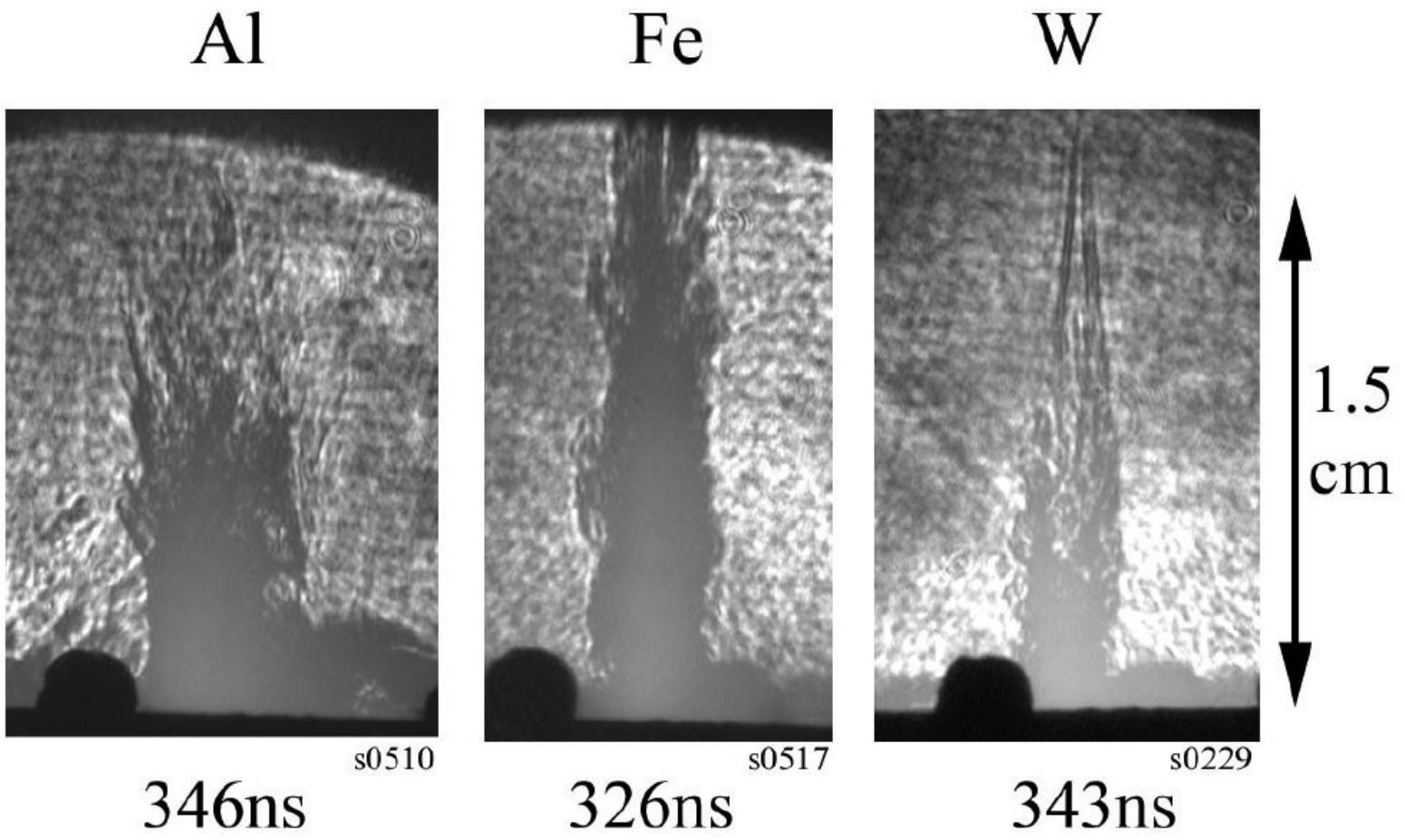

FIG. 3.—Laser probing images of plasma jets formed in aluminum, stainless steel, and tungsten wire arrays show that degree of collimation increases for elements with higher atomic number in which rate of radiative cooling is higher.

Lebedev et al.05, Hydrodynamic Propagation X-wind (Z-pinch/MAGPIE)

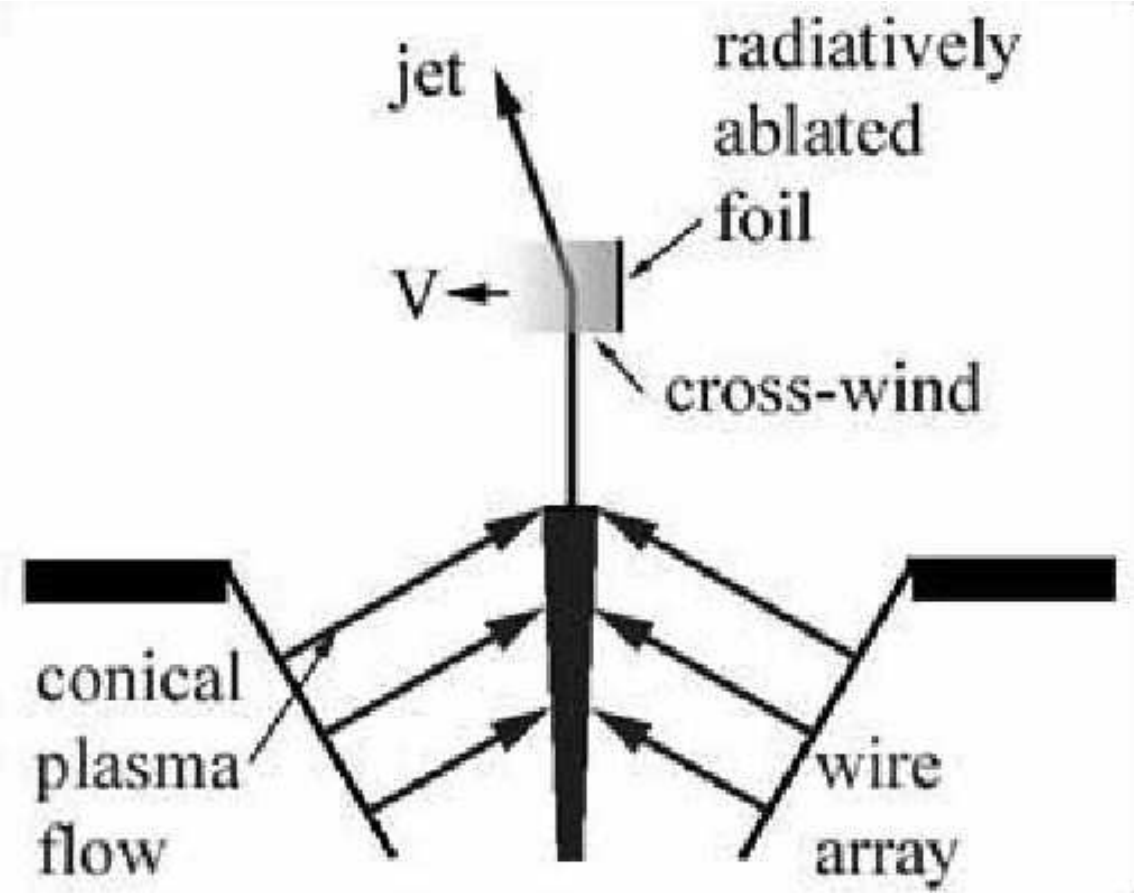

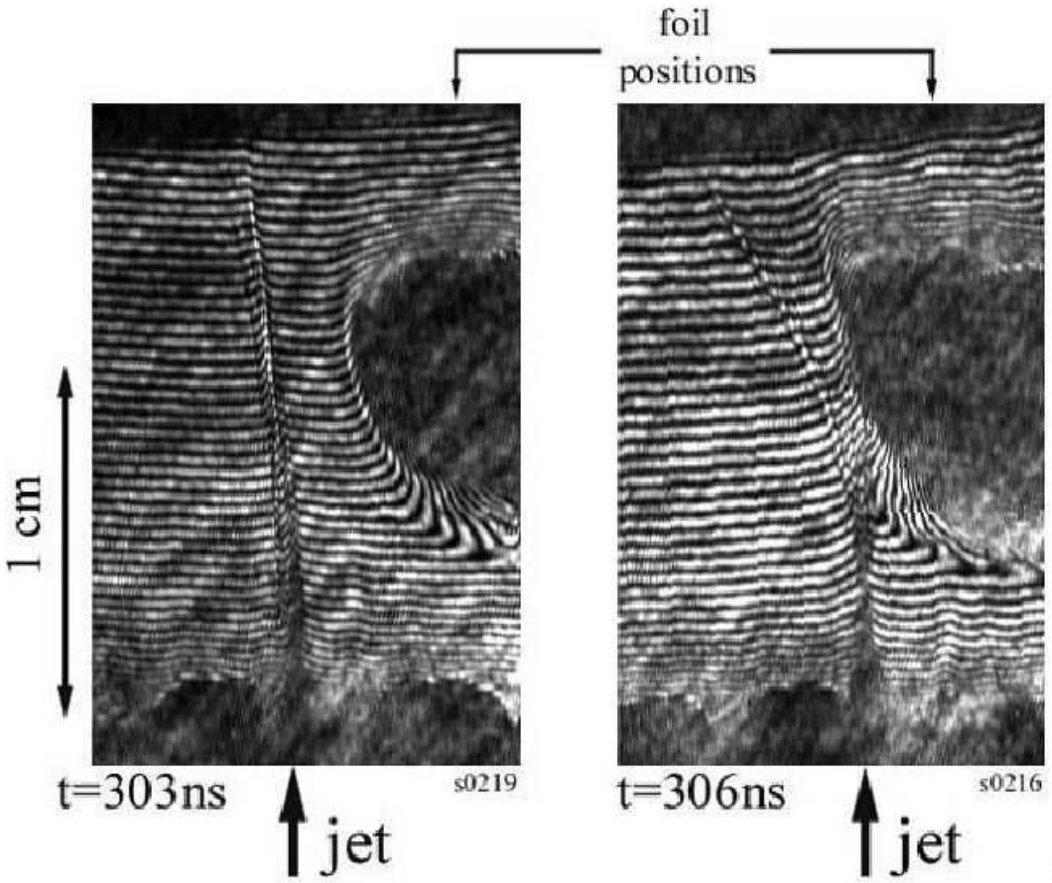

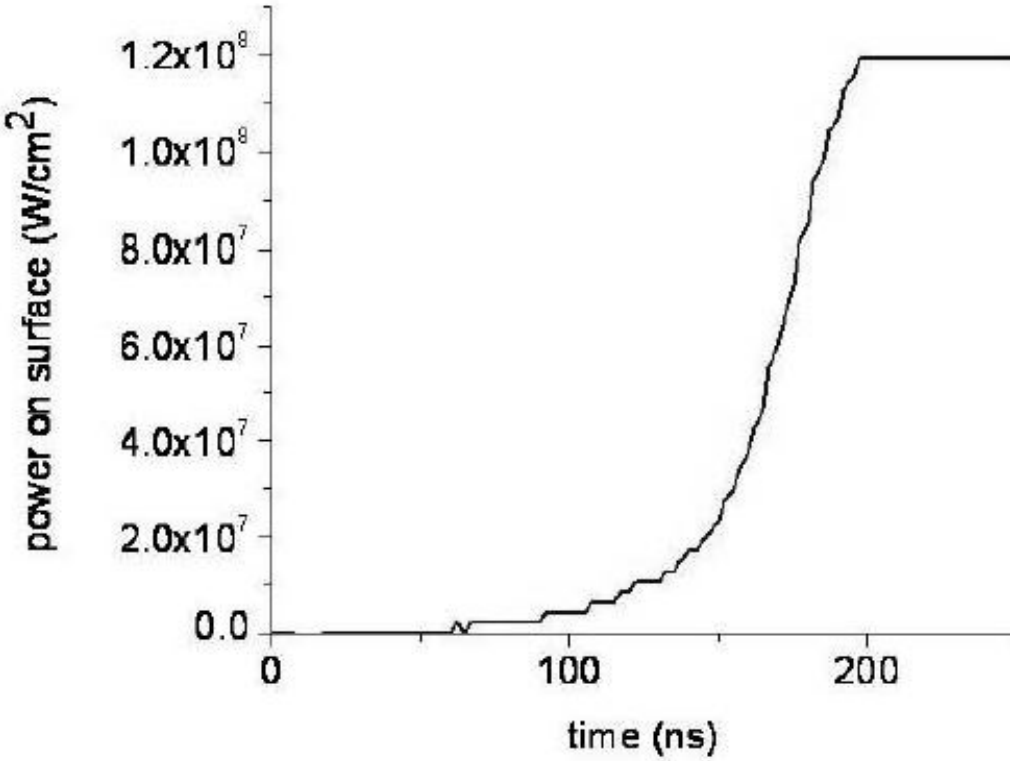

FIG. 5.—Power delivered via radiation to the surface of the foil that pro
duces the crosswind.

Insights from Lebedev et al.02 (cooling) & 04 (x-wind)

• Mach number ≥ 15 jets, $v_j \sim 200$km/s from converging conical flows

• Collimation by supersonic launch and cooling, consistent with Tenorio-Tagle,Canto et al. 1988

• Shock cloud interactions

• Stability to non-axisymmetric perturbations

• Shock crosswind interactions: internal and external shocks

• Code testing, 2-D vs 3-D effects, matching to exps, AMR Hydro code (ASTRO-Bear; Poludnenko et al 04)

Blue et al. 05 PROPAGATION EXP (NIF Laser ICF)

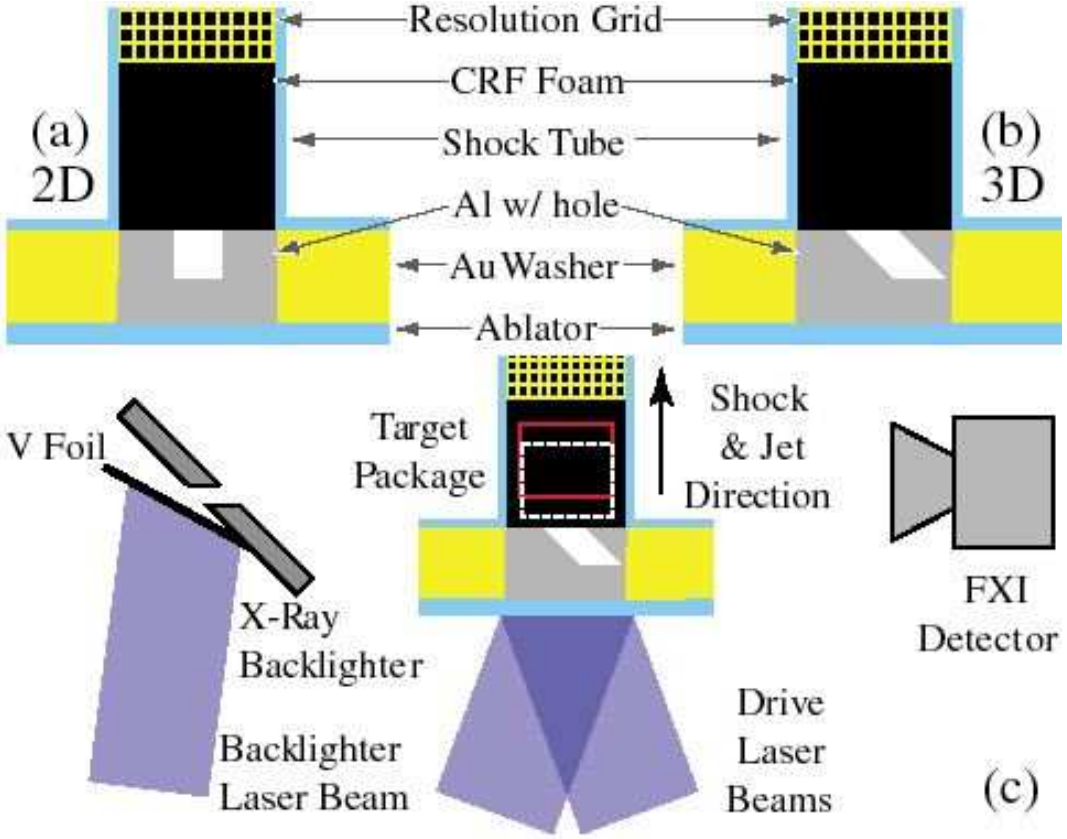

FIG. 1 (color). Schematic of a 2D target (a), a 3D target (b), and the radiographic configuration used on NIF (c) (not to scale).

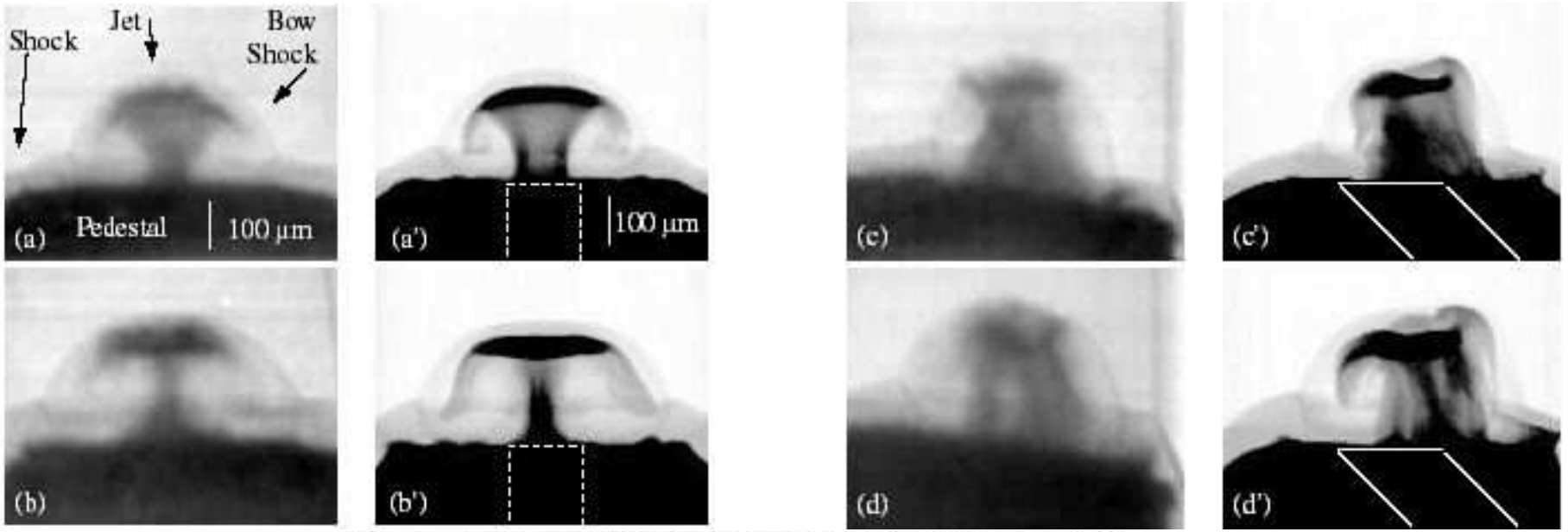

FIG. 2. Experimental and simulated radiographs of 2D and 3D jet targets. Experimental data are shown on the left (a)–(e) and the corresponding simulated radiographs are shown on the right (a′)–(e′). The 2D jet is shown at $t = 16$ (a),(a′) and 22 ns (b),(b′). The asymmetric view of the 3D jet is shown at $t = 16$ ns (c),(c′) and $t = 22$ ns (d),(d′). The symmetric view of the 3D jet at $t = 22$ ns is shown in (e),(e′). The dashed white lines in the simulated radiographs are the outlines of the preshocked holes offset upwards to the pedestal-foam interface.

Foster et al. 05 PROPAGATION (OMEGA/LLE Laser ICF)

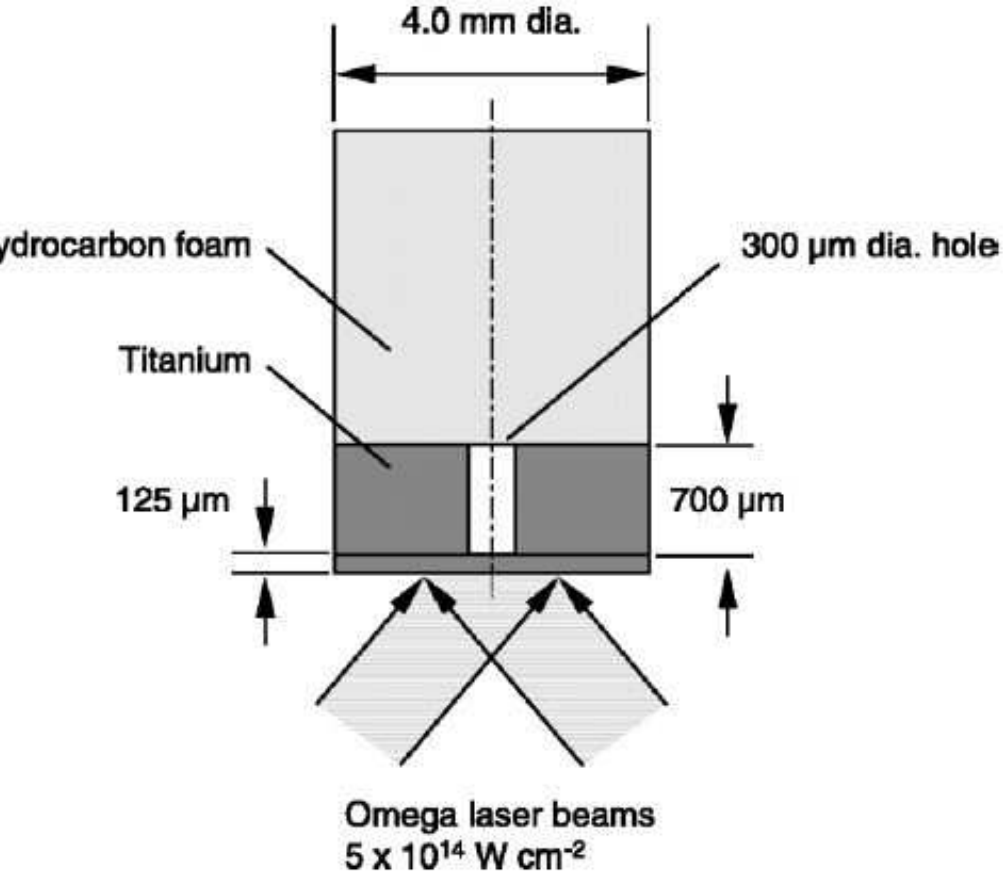

FIG. 1.—Experimental arrangement for the laser-driven supersonic-jet experiment. The laser target consists of a 4 mm diameter, 125 μm thickness titanium disk, in contact with a 700 μm thickness titanium "washer" with a central, cylindrical hole of 300 μm diameter. The face of the disk is illuminated by seven beams of the Omega laser, focused into a spot size of 0.6 mm diameter (50% intensity point). The laser pulse duration is 1 ns, with an incident intensity of 5×10^{14} W cm^{-2}; the incident intensity distribution is smoothed by random phase plates. The shock driven through this assembly produces a supersonic, dense-plasma jet that propagates into an adjacent cylindrical block resorcinol-formaldehyde ($C_{15}H_{12}O_4$) foam. This foam has a density of 0.1 g cm^{-3} and is chosen for its small cell size, $\lesssim$0.1 μm. The jet-foam interaction is diagnosed by point-projection radiography, using a 5.20 keV (He-like vanadium) backlighting source.

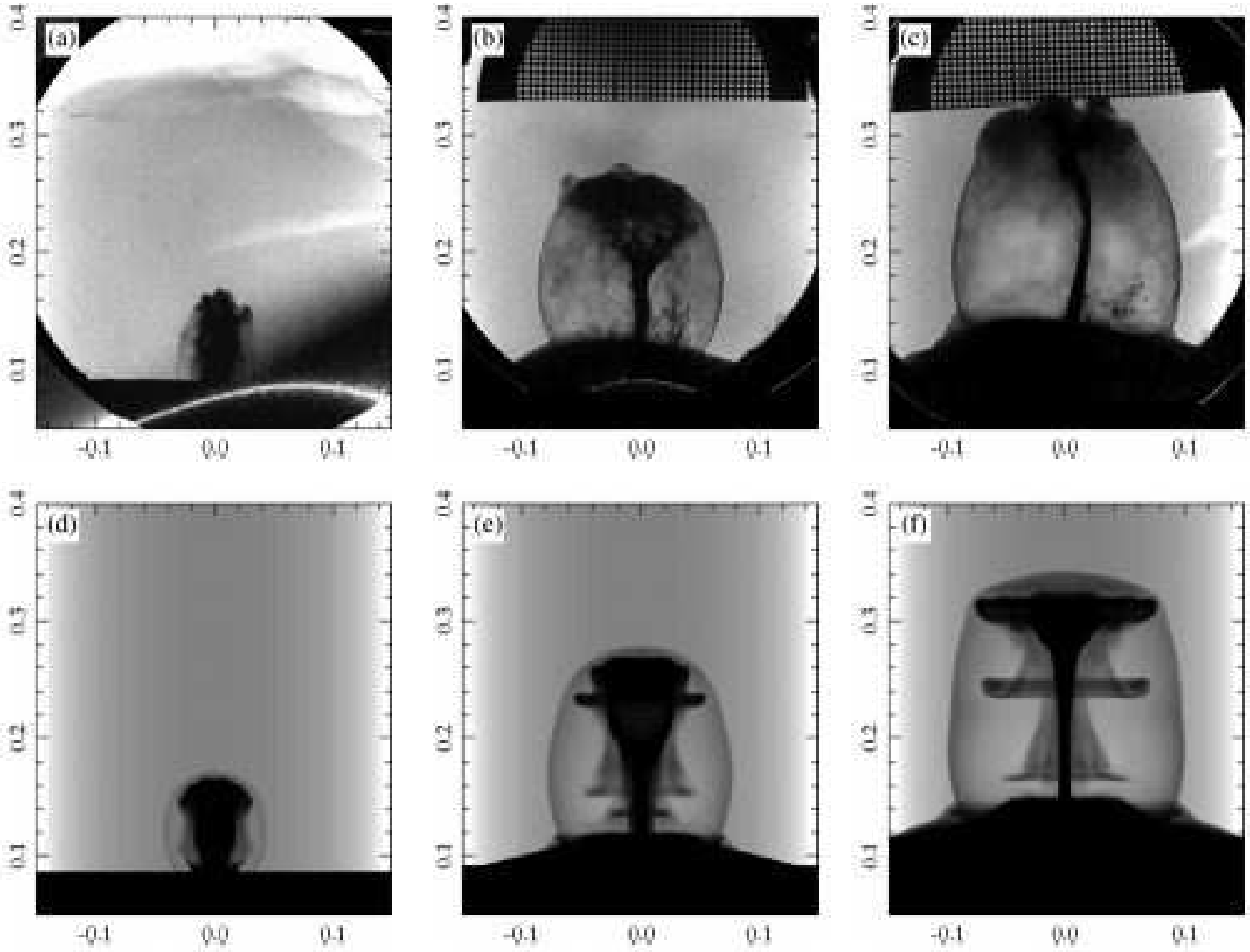

FIG. 2.—Experimental radiographs at (*a*) 100, (*b*) 200, and (*c*) 300 ns after the onset of the laser drive showing the primary (evident at 100 ns) and secondary (smaller diameter, evident at 200 ns and later) titanium jets. The dome-shaped pedestal results from shock transit through the titanium/foam interface. We also show transmission radiographs from simulations with RAGE in (*d*), (*e*), and (*f*). The diameters of the pedestal and jets, and the diameter of the bow shock in the low-density foam surrounding the jet, have been well captured, although a small offset and scaling of the times were necessary, which we attribute to small inaccuracies in the calculation of the pressure produced by the laser beams.

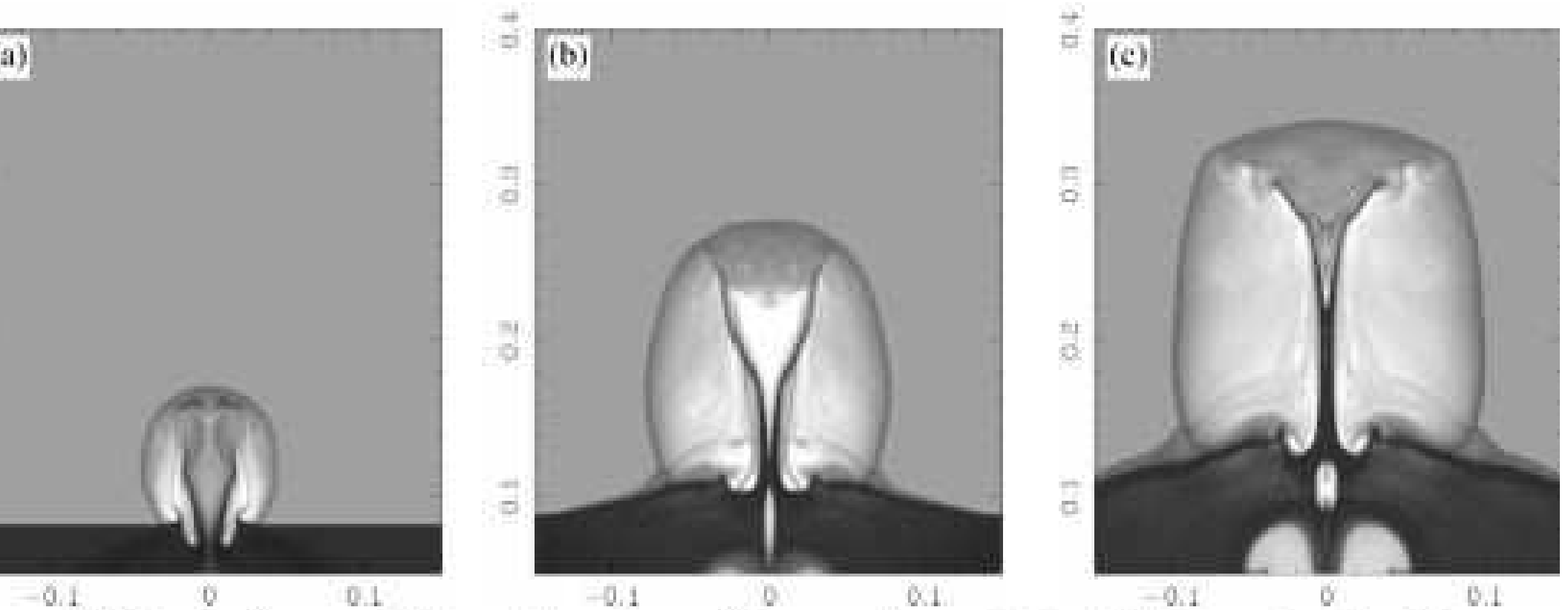

3.—Fluid density from the RAGE calculations at (*a*) 100, (*b*) 200, and (*c*) 300 ns. The gray scale is logarithmic, from 10^{-3} to 10^{13} gm^{-3}; the axes are
d in centimeters.

Insights from Blue et al.05; NIF jet propagation studies

• Probes aspects of propagation and effect of nozzle angle on jet structure: axial (2-D) vs. inclined nozzle (3-D)

• 3-D transits to turbulence faster than 2-D

• RT fingers also can be thought of as "jet" some insight into SN R-T fingers

• Insight into ICF target shape and effect of perturbation.

• Code testing, 2-D vs 3-D effects, 3-D radiative HD code HYDRA (Marinak et al. 96), but $R = 10^7$ in exp, $R = 10^2 - 10^3$ in sims.

Insights from Foster et al05 OMEGA propagation studies

• Probes aspects of jet propagation and shocks not formation
• Mach number $2 - 5$.
• Images clearer than in Blue et al. above
• Turbulent flow, dense plasma jets, bow shock structures.
• Code testing, 2-D HD RAGE (Gittings 1992) though other codes used also